Asian Journal of Chemistry; Vol. 30, No. 5 (2018), 988-992

ASIAN JOURNAL OF CHEMISTRY

https://doi.org/10.14233/ajchem.2018.21080

Synthesis of Graphene Oxide Nano Structures from Kerosene Soot and its Impedance Analysis

MASHIATH KHAN, POOJA JAYACHANDRAN and B. MANOJ*

Department of Physics and Electronics, Christ University, Bengaluru-560 029, India

*Corresponding author: E-mail: manoj.b@christuniversity.in

Received: 6 October 2017; *Accepted*: 31 January 2018; *Published online*: 29 March 2018; AJC-18826

Graphene oxide was synthesized from kerosene soot, by adapting three different treatments. The properties of each sample were studied using X-ray diffraction, UV-visible spectroscopy, FTIR and impedance measurements. The XRD results showed that the structural parameters (layer spacing, number of layers) were in agreement with expected values, indicating the reliability of kerosene soot as a precursor for graphene. The grain size was found to be small (1 to 2 nm) confirming the nanostructure of kerosene soot. The UV-visible spectra revealed high band gap even while conductivity was appreciably high. Other characteristic measurements showed frequency-independent conductivity, low resistance and low capacitance. FTIR spectra of all the treated samples and the precursor show the differences brought about in functionalization, due to the different methods of treatment. These differences, however, does not appreciably affect parameters such as band gap, conductivity and dielectric loss in any drastic way.

Keywords: Graphene oxide, Soot, Energy gap, Dielectric properties.

INTRODUCTION

Nanotechnology and nanocarbon has gained tremendous progress in recent years owing to their versatile properties. It broadly deals with the making, characterization and utility of materials, devices and systems with dimensions in the nano range, exhibiting significantly enhanced physical, chemical and biological properties. Investigation of different types of carbon nanostructures and graphene-forms the trending field in Material Science [1-4]. Hence, newer, simpler ways are being devised to synthesize this wonder material-graphene. Synthesis of graphene at a large scale is still a challenge, owing to the economy of the methods employed. In the present work, kerosene soot has been employed as the precursor for the synthesis of few-layered graphene oxide. Also, soot being one of the pollutants of the atmosphere, harnessing it and using it to produce a fine material such as graphene, would be an eco-friendly solution to the current needs. Dielectric measurements and conductivity studies have been reported for a wide variety of inorganic semiconductors. In nanocarbon materials such reported studies are scarce.

EXPERIMENTAL

Kerosene soot: Kerosene soot was prepared by burning kerosene in a glass bottle, with the help of a wick and collecting the product of the incomplete combustion (soot) on a tile. This black matter was then transferred to containers and labelled KS. The synthesis of few-layered graphene oxide was done through three different approaches –oxidation with nitric acid-sulphuric acid mixture, oxidation with nitric acid and hydrothermal treatment.

Oxidation with sulphuric acid-nitric acid mixture: The first method, involved introducing 0.5 g of the soot to a 3:1 mixture of sulphuric and nitric acids (30 mL and 10 mL, respectively). This mixture was sonicated for 2 h followed by magnetic stirring for 24 h at 80 °C. The mixture was diluted with 200 mL of water and was brought to room temperature. The mixture was titrated against the standard NaOH (1M) solution, till the mixture reached a neutral pH. The mixture was left to evaporate for 24 h. The resulting particulate matter was mixed in a minimum amount of water and sonicated and dialyzed for 24 h. The final product was dried at 75 °C (sample labelled KNS).

Oxidation with nitric acid: In the second method, 30 mL of nitric acid was used to treat 0.5 g of the precursor. The same process of sonication and stirring was carried out. The acidic content was washed with water, through continuous centrifugation at approximately 11000 rpm. The mixture was then centrifuged using acetone and dried. The dry sample was again washed with acetone, then added to water and sonicated and dialyzed. Finally, the residue was dried at 75 °C (sample labelled KNA).

Hydrothermal treatment: The last method was carried out by mixing 1 g of the precursor in 30 mL of water. The

mixture was sonicated for 2 h. It was then transferred to a Teflon container for hydrothermal treatment at 150 °C for 24 h. The furnace was removed and left to cool. The sample was further sonicated for 2 h. The sonicated sample was further treated in a microwave oven for 2 min (sample labelled KHT).

Characterization: The samples were characterized by X-ray diffraction analysis and the lateral size and stacking height were obtained using modified Scherrer formula [5].

Lateral size of the particles is given by:

$$L_a = \frac{1.84\lambda}{B_a \cos\delta}$$

The stacking height of the particles is given by:

$$L_c = \frac{0.89\lambda}{B_c \cos\phi}$$

where Ba and Bc are half widths of the peaks of the (100) and (002) planes δ and ϕ are the corresponding 2θ values for the peaks.

Measurements by impedance analyzer: The samples were analyzed by impedance analyzer under varying frequencies. The complex dielectric constant of the sample was calculated by:

$$\varepsilon(t) = \varepsilon'(t) - \varepsilon''(t)$$

where real dielectric constant is given by:

$$\varepsilon' = \frac{C_p \times t}{\varepsilon_o \times A}$$

where ε_o = permittivity of free space, t = thickness of sample/pellet, C_p = capacitance in parallel, A = area of the sample and the imaginary dielectric constant is given by:

$$\varepsilon'' = \frac{\varepsilon'}{\omega \times C_p \times R_p}$$

where ω = angular frequency, R_p = resistance in parallel.

Loss factor/loss tangent:

$$\tan(\delta) = \frac{\varepsilon''}{\varepsilon'}$$

AC conductivity of the sample is given by:

$$\sigma_{ac} = \omega \times \varepsilon_o \times \varepsilon' \tan(\delta)$$

RESULTS AND DISCUSSION

The X-ray profile of the synthesized samples are carried out and the results are presented in Fig. 1. The structural parameters are elucidated and depicted in Table-1.

The typical 2θ values for the sp^2 carbon forms of the (002) planes occur at approximately 25°, which constitutes the π band. However, there is a marked broadening of the peak, which can be attributed to the γ band, formed due to aliphatic side chains [2-6]. Lattice strain can also result in the broadening of the peak, but due to the small particle size, this effect is negligible. Some of the sharp, narrow peaks seen for KNA and KNS close to 30° can be due to nano-crystalline structures, which indicates that the sample is more varied when treated chemically, having sp^2-sp^3 carbon forms along with the crystalline forms, as opposed to a rather direct method used for KHT, where such peaks are not very noticeable.

The (100) peak occurs at approximately 44°, which is a common trait of these species. The lateral size ranges between 1 to 3 nm, with a stacking height of approximately 1 to 2 nm.

TABLE-1
STRUCTURAL PARAMETERS OF THE NANOSTRUCTURE FROM KEROSENE

Sample	L_a (nm)	L_c (nm)	d_o (Å)	N
KHT	1.3221	1.6514	3.5397	6
KNA	2.6808	1.1172	3.6021	4
KNS	2.0974	1.3023	3.5972	5

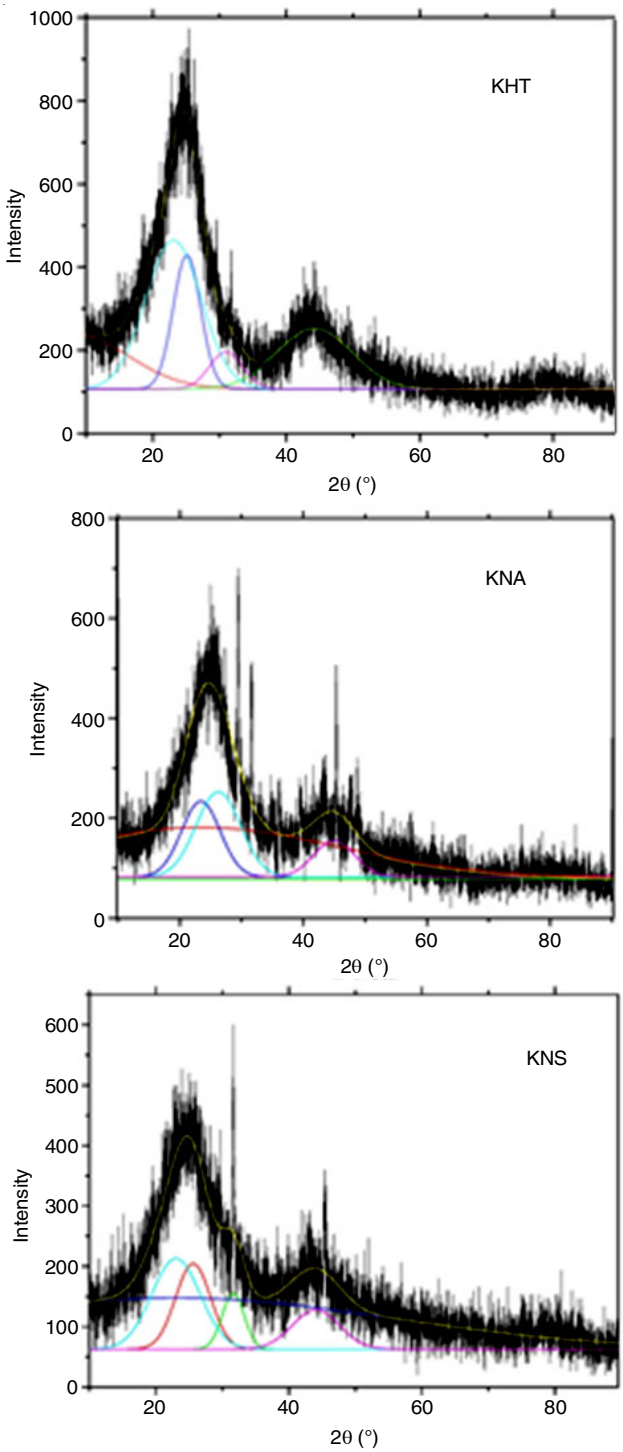

Fig. 1. X-ray analysis of the carbon nanostructure

The interlayer spacing is approximately 3.6 Å for KNA and KNS. For KHT, it is slightly lower at 3.5 Å. The number of layers is ranging between 4 and 6.

From the X-ray analysis, it is estimated that the synthesized carbon nano dots has roughly of 1 nm in size, with not more than 6 layers of carbon planes. These planes contain sp^2 carbons, which are also functionalized with sp^3 carbons.

UV-visible spectroscopy results: From the UV-visible spectra of the samples, there is a characteristic broad emphasis across the region, particularly between 250 nm to 500 nm, in all the samples. This indicates the π-π* transition, which clearly occurs at higher energies (not shown).

Also, the Tauc plots of the samples are obtained, considering that the band gap arises due to indirect allowed transitions (Fig. 2). In all the treated samples, as well as the precursor, the optical band gap ranges between 4.8 to 5.2 eV. This is a considerably high energy gap, which confirms the lower wavelength dependence for π-π* transitions.

FTIR analysis: The FTIR spectra (Fig. 3) indicate the clear presence of additional functional groups in the KNS and KNA samples. First, the sample KS shows C=C stretching at 1593 cm^{-1} indicative of cyclic alkene/aromatic ring and the presence of a slightly broad emphasis from 1200 to 1000 cm^{-1} showing that there are some C-O groups present before treatment as well. Since the trough is not sharp and lies in the fingerprint region, the nature of the C-O bond is rather indiscernible. A similar trend is seen in KHT, where no additional functional groups are observed.

However, in KNS a slightly sharper C-O trough at 1095 cm^{-1} is observed pointing towards a secondary OH group. This can also be attributed to C-N stretching, which happens in the same range. The C=C stretching trough can be seen much clearly here, at 1566 cm^{-1}. A medium intensity trough is seen at 3466 cm^{-1} which is due to N-H stretching. This N-H stretching in 3500-3400 cm^{-1} region is a sign of primary amines. There is also, a signal at 802 cm^{-1} which points to C=C alkene bending [5-9].

KNA sample has the highest degree of functionalization, have some characteristic features. The troughs of the C=C stretching at around 1600 cm^{-1} are deepened by the presence of N-O groups, as they have comparable bond transition energies. This fact can be confirmed by the presence of N-O stretching troughs present at two regions – at 1541 and 1373 cm^{-1}. The usual trend of C-O stretching is observed again around 1186 cm^{-1}, with the possibility that some C-N stretching might also contribute to the extended emphasis of the troughs. At 2354 cm^{-1}, there is another trough, which is attributed to carbon dioxide stretching. At 3386 cm^{-1} the trough corresponds to N-H stretching and the nature of the functional group is an aliphatic primary amine [7-12].

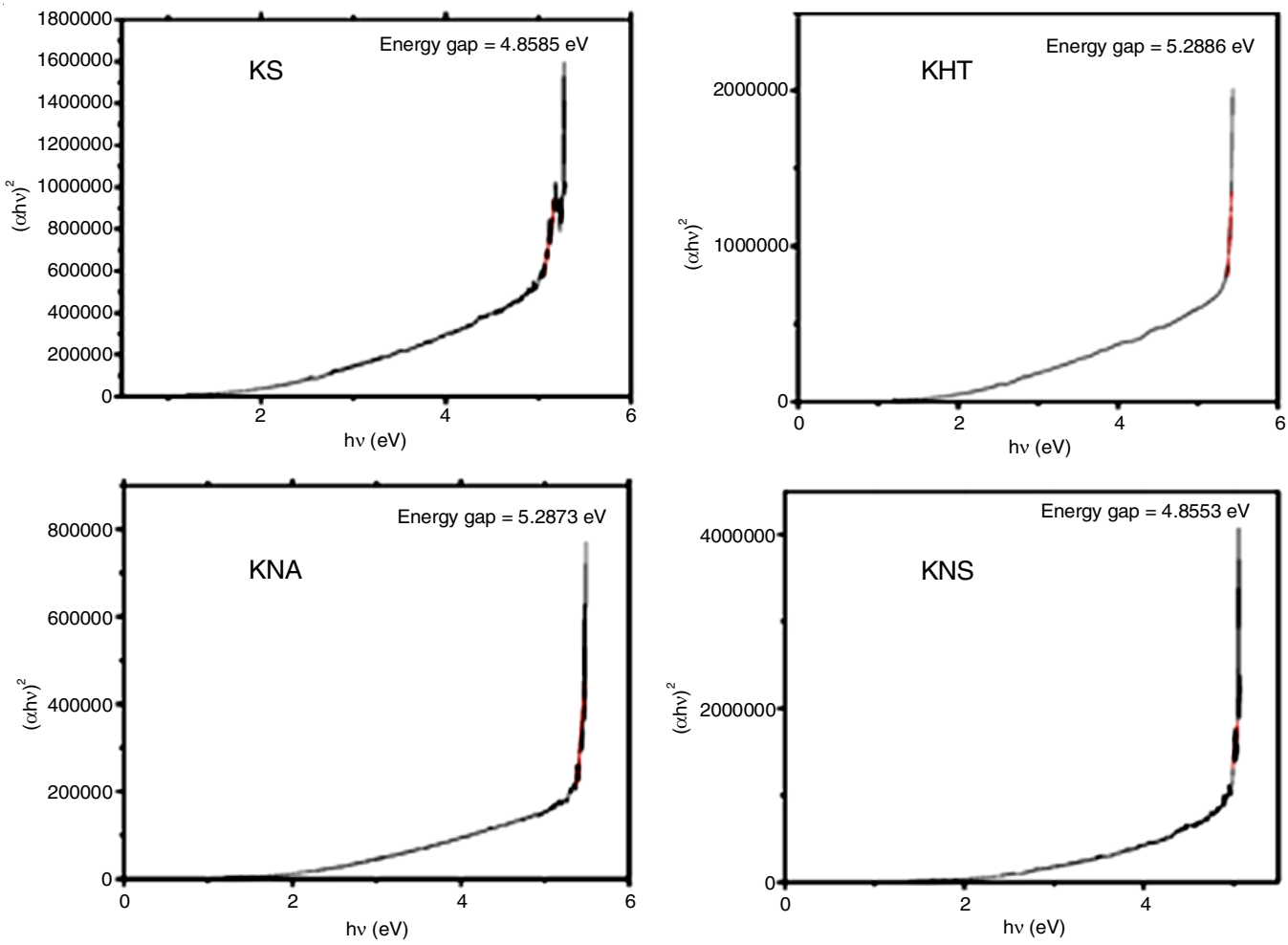

Fig. 2. Energy gap analysis of the nanocarbon from kerosene (Tauc plot)

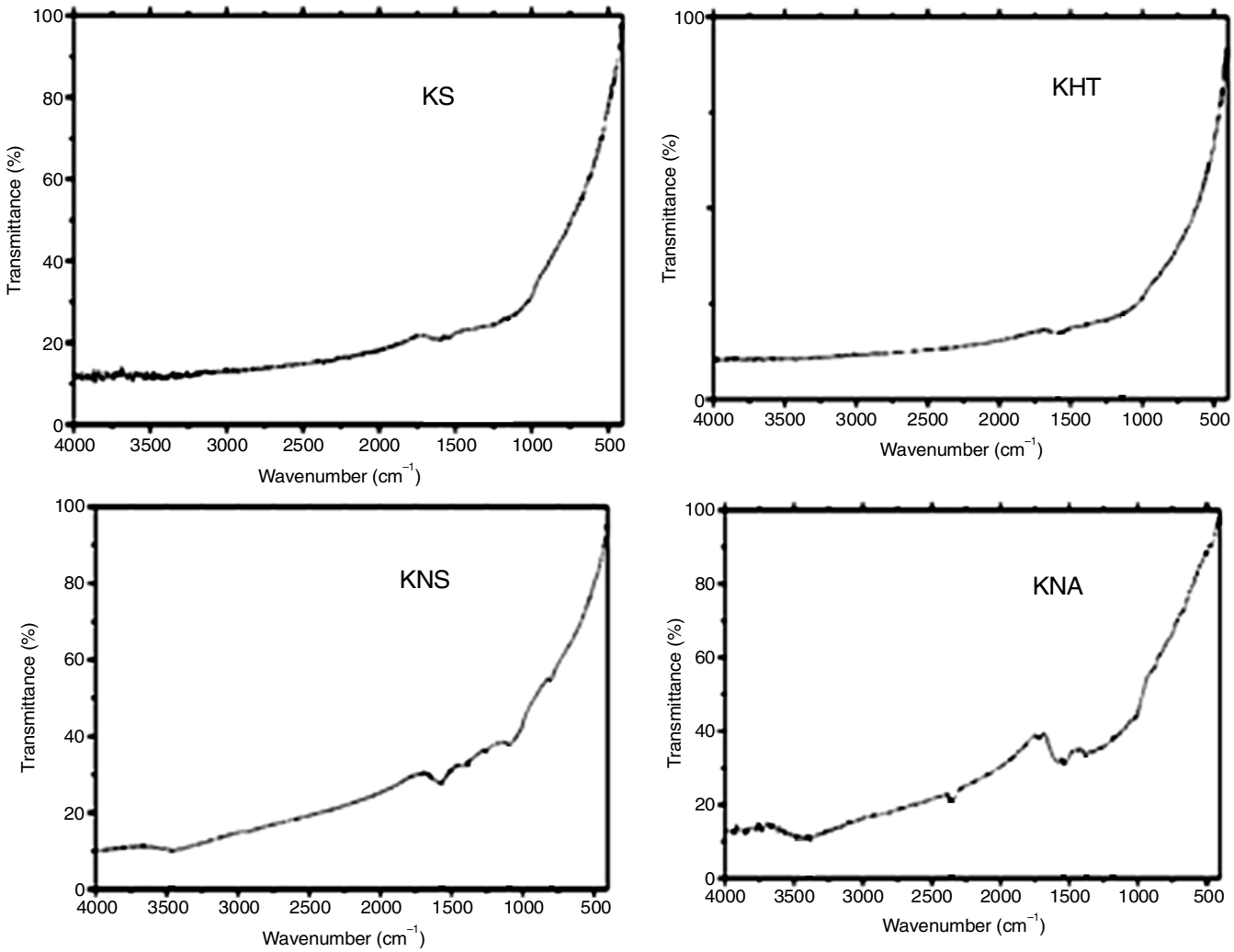

Fig. 3. FTIR analysis of carbon structure from kerosene

Impedance analysis

Dielectric properties: The variation in real part of the dielectric constant (ε′) and tan δ with frequency, for KNS and KNA nanostructure is presented in Fig. 4. For KNS, the real dielectric constant has a value of about 52 upto 20 kHz and decreases to around 37 at 0.65 MHz. In the case of KNA, the real dielectric constant has a value of about 26.8 upto 10 kHz, which decreases to about 25.8 at 0.6 MHz.

In both the cases, the value of the real dielectric constant decreases with increase in frequency and become frequency independent at high frequency. Space charge polarization can

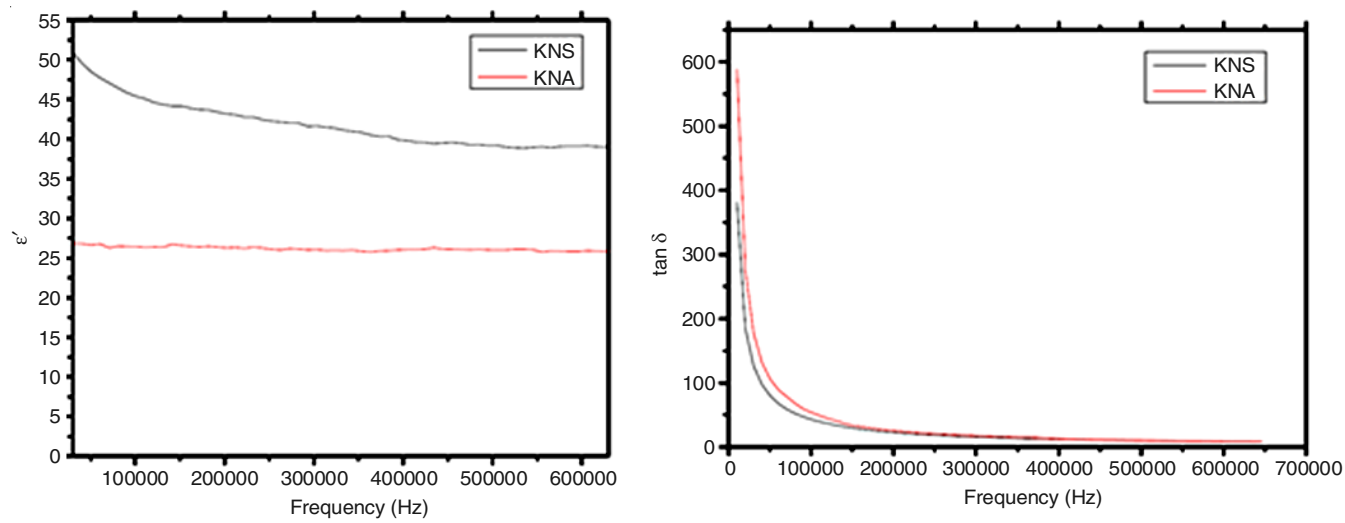

Fig. 4. Frequency dependence of (a) Real part of dielectric constant (ε′) and (b) dielectric loss (tan δ)

account for the higher values of ε′ at lower frequency. With increase in frequency, space charge polarization diminishes and electronic and atomic contribution dominates [13-16]. This is also the reason why the dielectric constant attains an almost constant value after a certain frequency (as the electronic and atomic contributions become most prominent).

On comparing KNA and KNS, KNA is found to have a lower value of ε′. It is known that higher the graphene concentration, lower the dielectric polarization and hence, lower the value of the real dielectric constant. Thus, it is possible that KNA has a greater graphene concentration than KNS. Also, since the dielectric constant of KNA attains a constant value almost immediately, it can be said that electronic and atomic contributions to dielectric constant are most prominent in KNA.

The dielectric loss or 'tan δ' represents the energy dissipation in the dielectric system. The above graph shows the variation of tan δ with frequency at room temperature. For KNA, the value of dielectric loss reaches a high of about 590 at low frequency and decreases to around 8 at 650 kHz. As for KNS, the value of dielectric loss starts at 382 at 10 kHz and also decreases to around 8 at 650 kHz. This shows that for both the samples, the value of dielectric loss decreases with frequency at room temperature. The high value of tan δ at lower frequencies can be attributed to space charge polarization, or in other words, accumulation of charges at the grain boundary [13-16]. This gives rise to high resistivity and hence higher dielectric loss.

The fact that the dielectric loss becomes constant for high frequency region makes the materials advantageous for use in high frequency device applications. It also indicates that the nanostructure has excellent optical quality with lesser defects.

AC conductivity studies: The AC conductivity is showing frequency independent behaviour for a wide range of frequency variation confirming that the hopping frequency is more or less constant (Fig. 5). From the above plots of frequency dependence of AC conductivity of KNS and KNA, it is clear that KNS sample has better frequency independent AC conductivity.

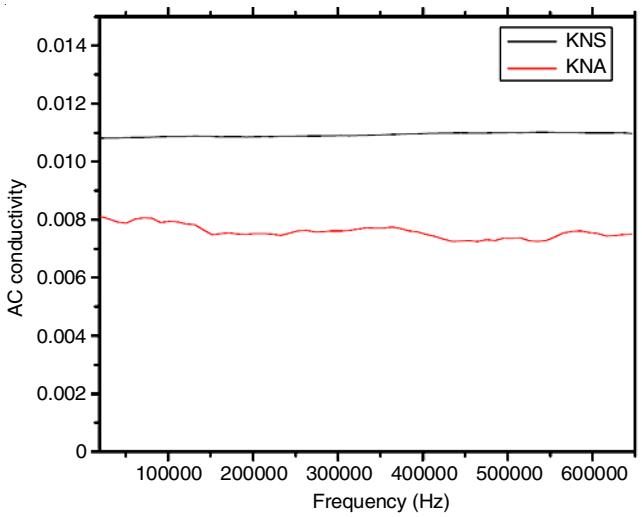

Fig. 5. Frequency dependence of AC conductivity (σ_{ac}) of the synthesized carbon structures

Conclusion

The XRD analysis of the obtained graphene oxide samples shows formation of nano structured dots with few layer. Further, from the UV-visible spectra, the π-π* transitions are seen to occur at higher energies. This is substantiated by the band gap obtained, which is markedly higher than that for semiconducting materials. The FTIR spectra show extensive functionalization in the samples KNA and KNS. These functional groups however, result in slight changes in electrical properties and band gaps. KNA has a higher band gap than KNS, while in the FTIR spectra, it is seen that it correspondingly has a higher degree of functionalization. The dielectric loss (tan δ) values are high at lower frequencies due to accumulation of charges at the grain boundary and the obtained species has charges that spend more time in one part of the grain, resulting in a higher equivalent series resistance, *i.e.*, higher dielectric loss. The AC conductivity is showing frequency independent behaviour for a wide range of frequency variation confirming that the hopping frequency is more or less constant. The values of the real dielectric constant decreases with increase in frequency and become frequency independent at high frequency. Space charge polarization can account for the higher values of ε′ at lower frequency.

REFERENCES

1. B. Manoj, *Asian J. Chem.*, **26**, 4553 (2014); https://doi.org/10.14233/ajchem.2014.15150.
2. A.V. Ramya, A.N. Mohan and B. Manoj, *Mater. Sci. Pol.*, **34**, 330 (2016); https://doi.org/10.1515/msp-2016-0061.
3. B. Manoj, *Russian J. Phys. Chem. A*, **89**, 2438 (2015); https://doi.org/10.1134/S0036024415130257.
4. A.A. Rao, A.M. Raj and B. Manoj, *Asian J. Chem.*, **29**, 2425 (2017); https://doi.org/10.14233/ajchem.2017.20722.
5. B. Manoj, *Int. J. Min. Met. Mater.*, **21**, 946 (2014).
6. A.V. Ramya, B. Manoj and A.N. Mohan, *Asian J. Chem.*, **28**, 1031 (2016); https://doi.org/10.14233/ajchem.2016.19577.
7. B. Manoj, *Int. J. Coal Sci. Technol.*, **3**, 123 (2016); https://doi.org/10.1007/s40789-016-0134-1.
8. B. Manoj, *J. Environ. Res. Dev.*, **9**, 209 (2014).
9. B. Manoj, M.R. Ashlin and T.C. Goerge, *Scientific Reports.*, **7**, 18012 (2017); https://doi.org/10.1038/s41598-017-18338-2.
10. B. Manoj, *Res. J. Biotechnol.*, **8**, 49 (2013).
11. B. Manoj and C.D. Elcey, *Res. J. Chem. Environ.*, **17**, 11 (2013).
12. B. Manoj, *J. Environ. Res. Dev.*, **6(3A)**, 653 (2012).
13. B.S. Rao, B.R. Kumar, V.R. Reddy, T.S. Rao and G.V. Chalapathi, *Chalcogenide Lett.*, **9**, 517 (2012).
14. I. Latif, T.B. Alwan, A.H. Al-Dujaili, *Nanosci. Nanotechnol.*, **2**, 190 (2012); https://doi.org/10.5923/j.nn.20120206.07.
15. T. Machappa, S. Manjunatha and A. Sunil Kumar, *Int. J. Sci. Technol. Manage.*, **4**, 714 (2015).
16. B.P. Prasanna, D.N. Avadhani, H.B. Muralidhara and M. Revanasiddappa, *Int. J. Latest Tech. Eng. Manag. Appl. Sci.*, **3**, 55 (2014).